New Type of Charge/Orbital Ordering above Room Temperature in the Perovskite $Bi_{2/3}Sr_{1/3}MnO_3$

M. Hervieu, S. Malo, O. Perez, P. Beràn, C. Martin, G. Baldinozzi,† and B. Raveau*

Laboratoire CRISMAT, UMR CNRS/ISMRA 6508, 6 bd du Maréchal Juin, 14050 Caen Cedex 4, France

Received September 23, 2002. Revised Manuscript Received November 11, 2002

A new type of charge ordering stable up to $T_1 \approx 500$ K has been evidenced by electron microscopy in the Mn^{3+}-rich perovskite $Bi_{2/3}Sr_{1/3}MnO_3$. This new superstructure, based on a *Imma*-type subcell is characterized by a double modulation with $a = 2a_p\sqrt{2}$, $b = 4a_p$, $c = a_p\sqrt{2}$. X-ray powder diffraction evidences a second structural transition at $T_2 \approx 580$ K and suggests a displacive modulation of the oxygen atoms below T_2. These results are interpreted as the correlated coexistence of charge-orbital ordering and modulated displacive ordering of oxygen atoms, in the form of double Mn stripes, below 500 K.

Introduction

The numerous studies carried out these last years on colossal magnetoresistance (CMR) manganites have shown the existence of complex structural transitions, despite the apparent simplicity of their perovskite structure. This is, for instance, the case of the charge order−disorder phenomena, which take place in the manganites $Ln_{1-x}Ca_xMnO_3$[1−7] and which play an important role in the appearance of the CMR effect. In these systems, charge ordering appears in the form of single Mn^{3+} stripes that alternate with multiple Mn^{4+} stripes, depending on x, resulting in incommensurate modulated structures. Charge-ordering phenomena are also observed in $Ln_{1-x}Sr_xMnO_3$ for $x \approx 1/2$ for a sufficiently small size of the lanthanide cation.[8,9] All of these oxides exhibit a $GdFeO_3$-type subcell "$a = a_p\sqrt{2}$, $b = 2a_p$, $c = a_p\sqrt{2}$, characterized by the *Pnma* space group, and charge ordering appears at low temperature, with a modulation vector qa^*, varying with the chemical composition x, i.e., with the Mn^{3+}/Mn^{4+} ratio.

The recent studies of the bismuth-based manganites show that the oxides $Bi_{1-x}A_xMnO_3$, with A = Ca and Sr, exhibit a different behavior.[10−17] Both oxides $Bi_{0.5}Ca_{0.5}MnO_3$ and $Bi_{0.5}Sr_{0.5}MnO_3$ exhibit charge ordering, but at much higher temperature, close to or above room temperature, i.e., $T_{CO} \approx 335$ and 530 K, respectively.[11,12] Similarly to the $Ln_{1-x}Ca_xMnO_3$ manganites, charge ordering is also observed for Mn^{4+}-rich compositions, as shown for $Bi_{1/3}Sr_{2/3}MnO_3$. Moreover, the electron diffraction (ED) study of these oxides shows that their original modulated charge-ordered structure, "$a = 1/qa_p\sqrt{2}$, $b = 2a_p$, $c = a_p\sqrt{2}$ with $q = 1/3$, involves a different subcell, namely, of the *Imma*-type. Their high-resolution electron microscopy (HREM) study[12] shows that their structure consists of double stripes of one sort of manganese Mn1 (likely Mn^{3+}) that alternates with double (for $x = 1/2$) or quadruple (for $x = 2/3$) stripes of a second sort of manganese Mn2 (likely Mn^{4+}).

The origin of these differences between the bismuth and lanthanide manganites is so far not understood. Bearing in mind these different results and the sensitivity of Bi-based phases to the thermal process, we have explored further the $Bi_{1-x}Sr_xMnO_3$ system, toward the Mn^{3+}-rich side. In the present paper, we show that the manganite $Bi_{2/3}Sr_{1/3}MnO_3$ is single-phased and exhibits a new type of superstructure up to 500 K, based on an *Imma* "$a_p\sqrt{2} \times 2a_p \times a_p\sqrt{2}$" subcell and characterized by a double modulation. HREM suggests that this superstructure originates from charge/orbital ordering (CO/OO) in the form of two sorts of Mn double stripes.

* To whom correspondence should be addressed.
† Present address: Ecole Centrale de Paris, Grande Voie des Vignes, 92295 Châtenay-Malabry Cedex, France.

(1) Schiffer, P.; Ramirez, A. P.; Bao, W.; Cheong, S. W. *Phys. Rev. Lett.* **1995**, *75*, 3336.
(2) Yonoki, S.; Moreo, A. *Phys. Rev. B* **1998**, *58*, 6403.
(3) . Dagotto, E. *Phys. Rev. Lett.* **1998**, *80*, 845.
(4) Martin, C.; Maignan, A.; Hervieu, M.; Raveau, B. *Phys. Rev. B* **2000**, *60*, 12191.
(5) Uhera, M.; Mori, S.; Chen, C. H.; Cheong, S. W. *Nature* **1999**, *560*, 399.
(6) Barnabé, A.; Maignan, A.; Hervieu, M.; Raveau, B. *Eur. Phys. J. B* **1998**, *1*, 45.
(7) Barnabé, A.; Martin, C.; Maignan, A.; Hervieu, M.; Raveau, B. *J. Appl. Phys.* **1998**, *84*, 5506.
(8) Woodward, P. M.; Okuda, T.; Tomioka, Y.; Asamitsu, A.; Tokura, Y. *Phys. Rev. Lett.* **1999**, *82*, 4316.
(9) Barnabé, A.; Hervieu, M.; Martin, C.; Maignan, A.; Raveau, B. *J. Phys. Chem. Solids* **2001**, *1365*, 62.
(10) Bokov, V. A.; Grigorian, N. A.; Bryzhina, H. F. *Phys. Status Solidii* **1967**, *20*, 745.
(11) Garcia-Munoz, J. L.; Frontera, C.; Aranda, M.; Llobet, A.; Ritter, C. *Phys. Rev. B* **2001**, *63*, 64415.
(12) Hervieu, M.; Maignan, A.; Martin, C.; Nguyen, N.; Raveau, B. *Chem. Mater.* **2001**, *13*, 1356.
(13) Beran, P.; Malo, S.; Martin, C.; Maignan, A.; Nevriva, M.; Hervieu, M.; Raveau, B. *Solid State Sci.* **2002**, in press.
(14) Frontera, C.; Llobet, A.; Garcia-Aranda, M. A.; Ritter, C.; Garcia-Munoz, J. L. *Phys. Rev. B* **2000**, *276*, 794.
(15) Murakami, Y.; Shindo, D.; Chiba, H.; Kikuchi, M.; Syono, Y. *Phys. Rev. B* **1997**, *55* (22), 15043.
(16) Su, Y.; Du, C. H.; Hatton, P. D.; Collins, S. P.; Cheong, S. W. *Phys. Rev. B* **1999**, *59* (18), 11687.
(17) Santosh, P. N.; Goldberger, J.; Woodward, P. M.; Vogt, T.; Lee, W. P.; Epstein, A. J. *Phys. Rev. B* **2000**, *62*, 14298.

10.1021/cm021309f CCC: $25.00
Published on Web 12/31/2002

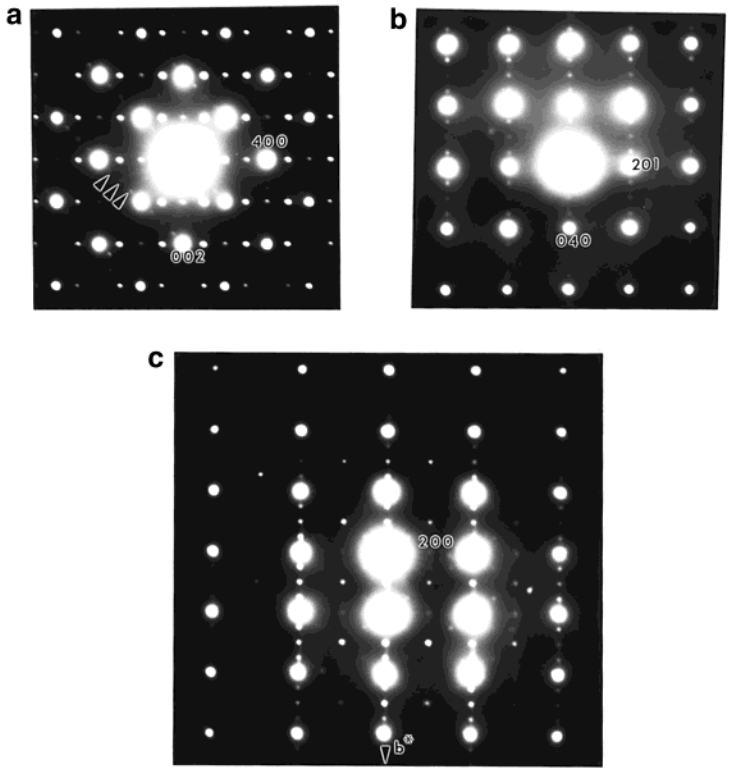

Figure 1. $Bi_{2/3}Sr_{1/3}MnO_3$ ED patterns recorded at room temperature: (a) [010], (b) $[10\bar{2}]$, and (c) [001]. They are indexed in the $a = 2a_p\sqrt{2}$, $b = 4a_p$, $c = a_p\sqrt{2}$ supercell. The weak reflections indicated by the black arrows are due to a twinning effect.

Moreover, X-ray powder diffraction (XRPD) data evidence a second structural transition at $T_2 = 580$ K.

Experimental Section

Polycrystalline $Bi_{2/3}Sr_{1/3}MnO_3$ was prepared starting from SrO_2, Bi_2O_3, and Mn_2O_3, in stoichiometric ratios. The mixture was ground in an agate mortar, pressed in the form of bars (2 × 2 × 10 mm^3) and sealed in an evacuated silica tube. The sample was heated at 1100 °C for 12 h, increasing and decreasing the temperature for 6 h.

The sample was characterized by XRPD at room temperature using a Philips diffractometer, working with Cu Kα in the range $10° \leq 2\theta \leq 100°$. The sample for transmission electron microscopy was crushed in alcohol, and the small flakes were deposited on a holey carbon film, supported by a copper grid. The reconstruction of the reciprocal space was carried out at room temperature with a JEOL 200 CX electron microscope. The ED study versus temperature was carried out from 90 to 500 K, using a JEOL 2010 electron microscope, equipped with an energy-dispersive spectroscopy (EDS) analyzer. HREM was carried out at room temperature with a TOPCON 002B electron microscope (working at 200 kV, spherical aberration constant $C_s = 0.4$ mm).

XRPD patterns were also collected up to $2\theta = 140°$ on a high-accuracy microcontrol diffractometer using Cu Kβ radiation and a rotating anode generator of 18 kW. The records at 80 and 473 K were performed in a flowing cryostat. A furnace was used to collect data at high temperature in air. Data collection conditions have been optimized to improve the peak-to-background ratio. Structural refinements were carried out using the Rietveld method[18] (20 structural parameters are refined for 138 *hkl* reflections). Differential scanning calorimetry measurements were performed using a Seiko DSC 220C microcalorimeter. The sample (≈32 mg) was loaded in an aluminum crucible, and Al_2O_3 was taken as a reference. Scans on heating and on cooling were performed in the range 293−723 K at a temperature rate of 3 K min^{-1}.

(18) Program XND: Berar, J. F.; Garnier, P. APD 2nd Conference NIST, May 1992, Gaithersburg, MD.

Results and Discussion

Following the aforementioned thermal process, the XRPD patterns recorded vs T exhibit the intense characteristic reflections of the perovskite-like phases. The EDS analysis of numerous crystallites shows that the title sample is very homogeneous with the cationic composition "$Bi_{0.67(2)}Sr_{0.33(2)}Mn_1$". No secondary phase could be detected from the ED observations, in agreement with the XRPD patterns.

The ED investigation at room temperature shows that the intense reflections are those of a perovskite structure but evidences the presence of a complex system of extra reflections, characteristic of a double modulation. The perovskite subcell is orthorhombic with $a_I = a_p\sqrt{2}$, $b_I = 2a_p$, $c_I = a_p\sqrt{2}$, and the space group is *Imma* (a_p is the parameter of the ideal single perovskite cell, and the suffix I refers to the I-type subcell). The extra reflections (Figure 1) imply an orthorhombic supercell with $a = 2a_p\sqrt{2}$, $b = 4a_p$, $c = a_p\sqrt{2}$; it must be outlined that they are rather intense, as illustrated by the intermediate $[\bar{1}01]$ ED pattern given in Figure 2a. The [010] and $[10\bar{2}]$ ED patterns of the new supercell, which are equivalent to the $[010]_I$ and $[101]_I$ patterns of the subcell, are given in parts a and b of Figure 1, respectively, and the [001] ED pattern is given in Figure 1c. The reconstruction of the reciprocal space shows that there are no conditions limiting the *hkl* reflections, but the *hk*0 reflections with $h = 2n + 1$ are scarcely or not visible.

Most of the crystallites exhibit twinning domains. These domains are systematically observed in the

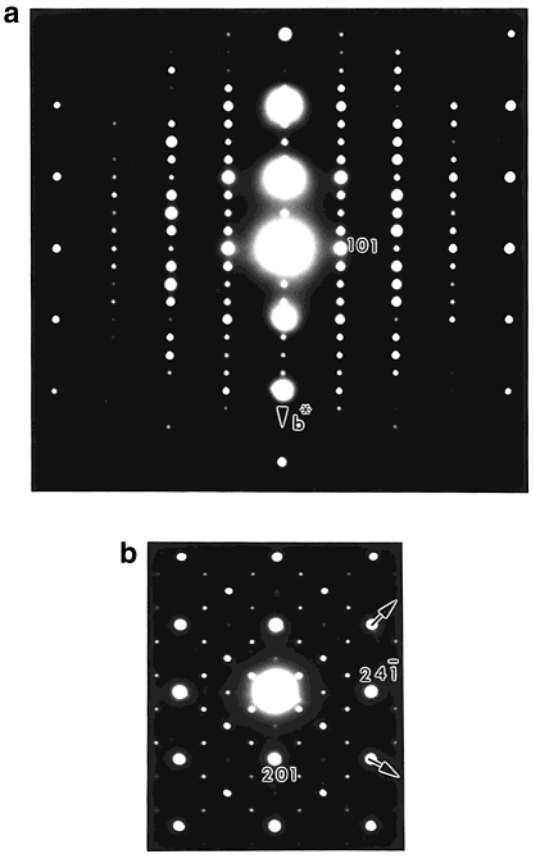

Figure 2. (a) [10$\bar{1}$] ED pattern showing the rather intense system of extra reflections in the reciprocal space. (b) Typical ED pattern showing the coexistence of the [$\bar{1}$12] variants (the black arrows indicate the [111]* direction and the other extra reflections result from double diffraction phenomena).

Pnma- and *Imma*-type $Ln_{1-x}A_xMnO_3$ perovskites as a result of the orthorhombic distortion. All of the possible variants of the *Imma* parent structure are observed in the supercell, explaining the complexity of some ED patterns. A first example is observed in the [010] ED pattern of Figure 1a, where weak additional reflections, indicated by the three small black arrows, are the signature of a superimposed [10$\bar{2}$]-oriented domain. The second example in Figure 2b shows a typical ED pattern, where the [$\bar{1}$12] variants coexist (see the two black arrows which indicate the [111]* directions).

The ED patterns, registered at low temperature, from 92 to 300 K, do not allow any structural change to be detected. The ED patterns registered at high temperature show that by increasing T from 300 to 520 K the satellites remain at the same positions but their intensities decrease. At about 450 K the satellites along the [100]* direction are no more visible, whereas those along the [010]* direction are very weak but still visible. Above 500 K, all of the satellites have disappeared and the conditions of reflection are those of the *Imma*-type structure.

The important information displayed by XRPD patterns, registered from 80 to 723 K, is the absence of extra reflections with respect to the *Imma* "$a_p\sqrt{2} \times 2a_p \times a_p\sqrt{2}$" subcell, indicating clearly that the superstructure does not originate from an ordering of the Bi^{3+} and Sr^{2+} species. The evolution of the subcell parameters versus temperature (Figure 3a) shows that they increase continuously as T increases up to 580 K. More

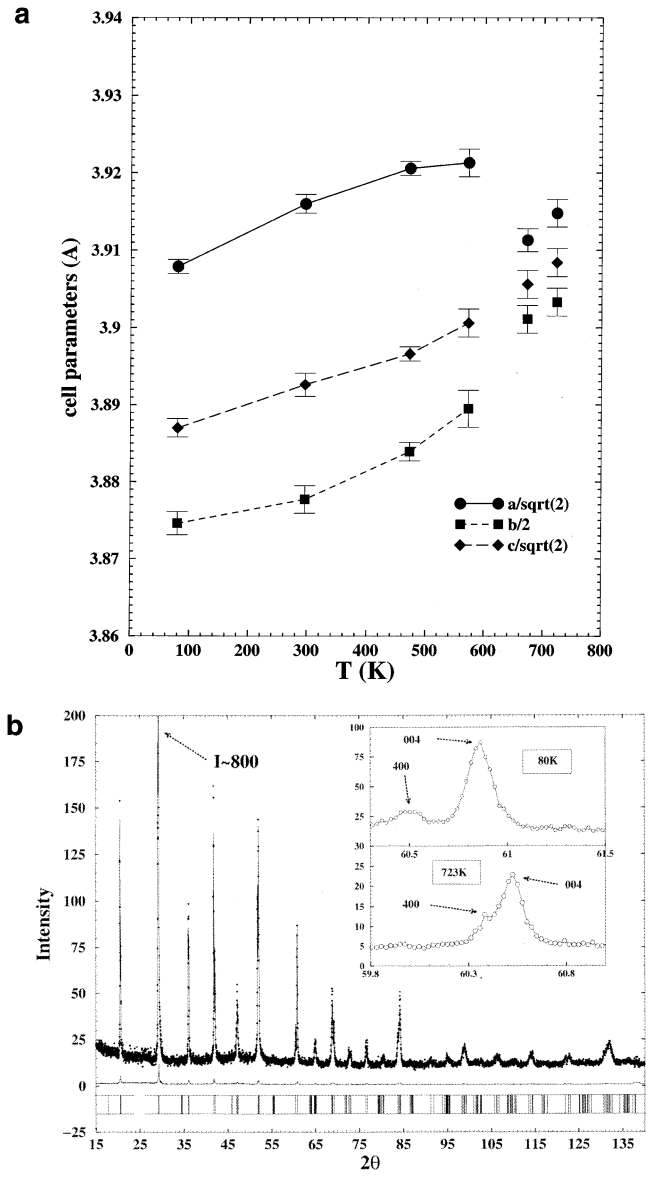

Figure 3. Powder XRD data: (a) evolution of the subcell parameters versus temperature; (b) X-ray diffraction pattern and enlargement of the 400 and 004 reflections at $T = 723$ and 80 K, allowing one to discard a tetragonal cell for the high-temperature form of $Bi_{2/3}Sr_{1/3}MnO_3$. The experimental points, calculated pattern, and difference curve are drawn.

particularly, at 500 K, which is the temperature of the satellites vanishing in the ED patterns, no transition is detected (collected on the same sample). An abrupt decrease of the orthorhombic distortion appears beyond 580 K. However, a transition from orthorhombic to tetragonal symmetry is ruled out, as shown, for example, from the splitting of the 400 and 004 reflections observed at 723 K on the XRPD pattern (Figure 3b). The DSC measurements show a peak at 581 K on heating and at 577 K on cooling (Figure 4), which corresponds to a structural transition in agreement with T_2 determined from the XRPD patterns. In the same way, no signal is detected around 500 K, in relation with the disappearance of the extra reflections on the ED patterns. The refinement of the structure from XRPD data, using the *Imma* "$a_p\sqrt{2} \times 2a_p \times a_p\sqrt{2}$" subcell, although it cannot be considered as very accurate, brings additional information. The refined coordinates

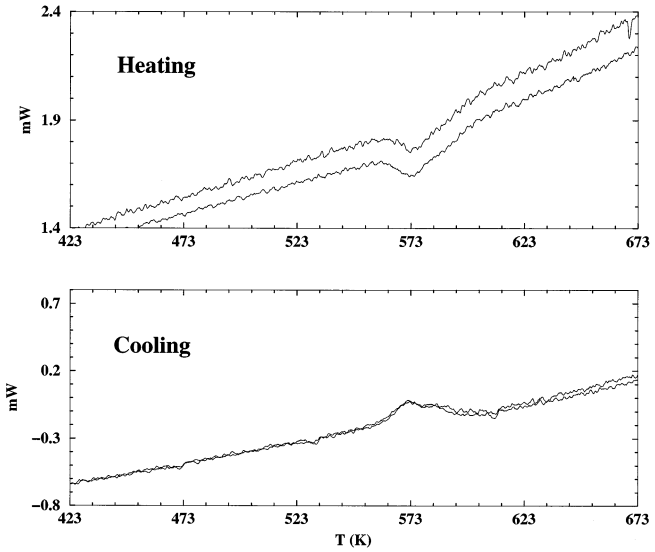

Figure 4. DSC measurements showing a peak at 581 K on heating and at 577 K on cooling.

Table 1. XRPD Data of $Bi_{2/3}Sr_{1/3}MnO_3$: (a) *R* Values Obtained from the Refinements vs *T*; (b) Anisotropic Displacement Parameters Refined at 298 K; (c) Positional Parameters in the *Imma* Space Group[a]

	80 K	298 K	473 K	573 K	673 K	723 K
R_{Bragg} (%)	6.3	8.1	8.4	7.3	7.4	5.8
R_{wp} (%)	8.4	7.4	5.6	8.2	5.5	6.8
R_F (%)	5.2	7.6	7.4	8.2	9.9	6.9

	U_{11} (Å^2)	U_{22} (Å^2)	U_{33} (Å^2)	U_{12} (Å^2)	U_{13} (Å^2)	U_{23} (Å^2)
Bi/Sr	0.022(2)	0.015(2)	0.026(3)		0.008(3)	
O1	0.010(3)	0.016(4)	0.16(8)		0.010(5)	
O2	0.028(8)	0.014(4)	0.07(2)		0.020(4)	
O3	0.056(2)	0.06(2)	0.03(1)			0.04(3)

Bi/Sr	0	0	$^1/_2$
Mn	0	$^3/_4$	0
O1	$^1/_4$	$^1/_4$	$^1/_4$
O2	$^1/_4$	$^3/_4$	$^1/_4$
O3	0	0	0

[a] The *Imma*-type structure can be described from two different origins. The first possibility with Mn in $00^1/_2$ involves two independent oxygen positions, while the second one with Bi in $00^1/_2$ leads to three special positions for the oxygens. All of the XRPD refinements converge on a single solution with special positions for all of the atoms.

obtained at 80 K (Table 1) confirm the absence of ordering between Sr^{2+} and Bi^{3+} species. More importantly, the anisotropic displacement parameters (Table 1) show large oxygen displacements for O1, O2, and O3 along the *c* axis, in the (*a*, *c*) and (*a*, *b*) planes, whereas small displacements are observed for Bi/Sr. These values of the thermal factors may correspond to modulated displacements of the oxygen atoms with respect to their ideal positions in the *Imma* subcell. Such a modulated ordering of the oxygen atoms would bring a too small contribution to the structure factors to be detected from XRPD data.

For the HREM study, the [010] and [001] directions were especially selected for gathering information on the modulated structure along $\vec{a}$ and $\vec{b}$. The focus values were systematically recorded for each of them. A typical [010] HREM image, recorded for a focus value where the cation positions are highlighted (focus close to −55 nm), is shown in Figure 5. The theoretical images calculated for the parent *Imma* structure, using the

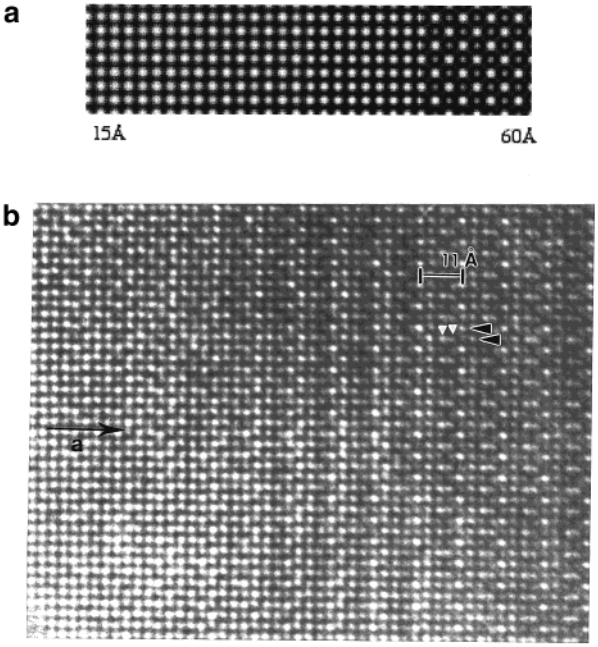

Figure 5. (a) Parent *Imma* structure: theoretical [010] HREM images calculated for a crystal thickness varying between 15 and 60 Å (focus close to −55 nm). (b) Corresponding experimental image showing the contrast in double stripes for a contrast where the high electron density areas are highlighted. The two types of double rows are differentiated by black and white small triangles.

positional parameters given in Table 1, show that the two types of cations, namely, "$Bi_{0.67}Sr_{0.33}$" and "Mn", can hardly be differentiated in the very thin edge of the crystallite (see Figure 5a, for a thickness of 15 Å), but a clear difference is observed for a crystal thickness of a few nanometers (see for a crystal thickness of 60 Å), where the ($Bi_{0.67}Sr_{0.33}$) cations appear as the brighter dots and the Mn cations as the less bright ones, arranged in staggered positions along a_I and c_I. In the experimental images, the contrast also quickly evolves with the crystal thickness, but the staggered array of dots, characteristic of the parent structure, is only observed for two adjacent rows out of four parallel to $\vec{c}$. Along $\vec{a}$, the modulation generates a contrast in the form of double rows characterized by two types of bright dot arrangements. The first type is made of two adjacent rows of staggered dots (see black triangles in Figure 5) and the second one of two adjacent rows of dots of equal brightness at the same level but alternating bright and less bright along $\vec{c}$ (see white triangles in Figure 5). The series of images where the cation positions are highlighted confirm the absence of ordering between Bi and Sr and are in favor of differences in the cation environments. For the focus values (close to −35 nm) where the oxygen positions are highlighted (Figure 6), the "double rows"-type contrast is also observed but the main information is the important shifting of the bright dots (with regard to the average positions of the *Imma* subcell) along the direction perpendicular to the modulation vector. The waving effect is especially visible by viewing at glazing incidence along $\vec{c}$ and is enhanced by the irregular spacing of the bright dots along the rows (see the small **s** and large **L** interdot distances indicated by arrows in Figure 6). Figure 7 presents [001] (left part of the image) and [$\bar{1}$12] (right part) twinning

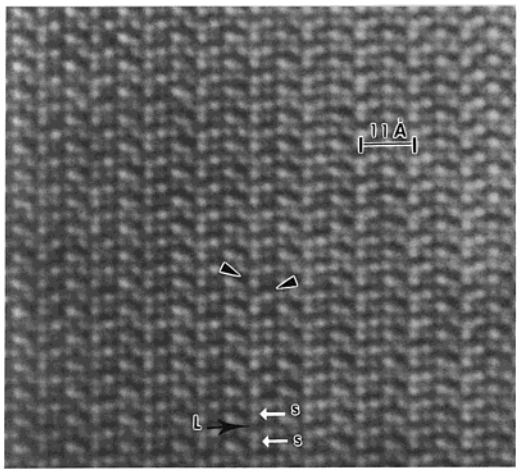

Figure 6. Experimental image recorded for a focus value close to −35 nm. It shows the important shifting of the bright dots with regard to the average positions of the *Imma* subcell. The L and s letters show the variation of the inter-dots distances along a direction perpendicular to the modulation vector.

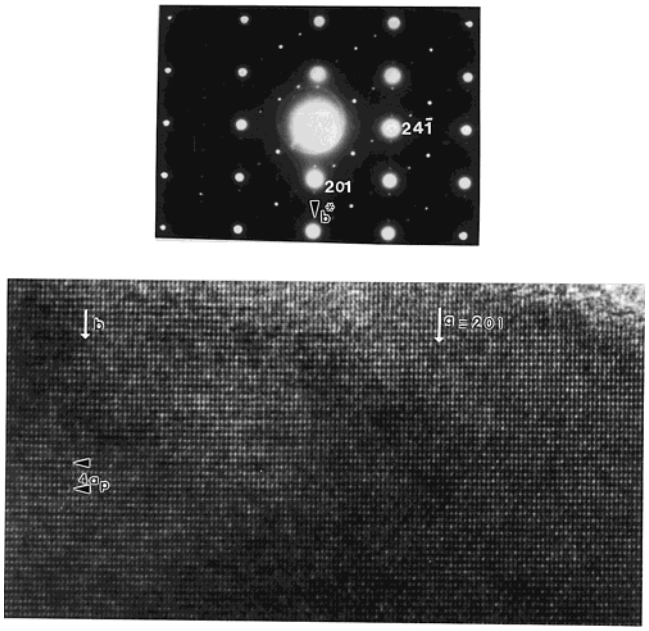

Figure 7. ED pattern and HREM image of winning domains in $Bi_{2/3}Sr_{1/3}MnO_3$ oriented along [001] in the left part of the image and along [$\bar{1}$12] in the right part. The modulated contrast results from complex and irregular variations of the brightness and dot displacements in the whole space.

zones; they both show complex and irregular variations of the brightness and dot displacements over $4a_p$ in the whole space so that, clearly, the images recorded along [010] cannot be simply interpreted as in a perovskite subcell. However, the "double rows"-type contrast is likely correlated to the existence of differently distorted MnO_6 octahedra. It is to be compared to that observed in $Bi_{0.5}Sr_{0.5}MnO_3$[12] and suggests a charge/orbital ordering phenomenon, in the form of double stripes of manganese of one sort (labeled Mn1) alternately with double stripes of a second sort (Mn2), as exemplified in Figure 8. Thus, a polaronic ordering can be proposed on one sort of double row of (Mn1) octahedra, which would mainly contain "Mn^{3+}" and, consequently, would be more distorted because of the Jahn−Teller effect, whereas the second sort (Mn2) would be mixed-valent Mn^{3+}/Mn^{4+} and then less distorted.

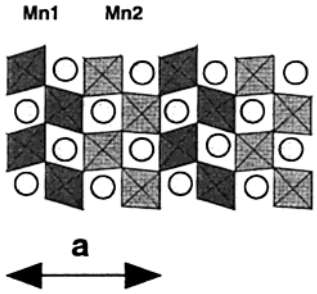

Figure 8. Hypothetical idealized "*double rows*" model, based on two sorts of octahedra Mn1 and Mn2, differently distorted.

Concluding Remarks

In this study, a new type of superstructure which disappears above $T_1 = 500$ K has been evidenced in the manganite $Bi_{2/3}Sr_{1/3}MnO_3$. The first remarkable feature of this manganite deals with the analogy of its superstructure with that observed for $Ln_{0.5}Ca_{0.5}MnO_3$,[1−7] $Ln_{0.5}Sr_{0.5}MnO_3$,[8,9] and $Bi_{0.5}A_{0.5}MnO_3$ with A = Ca and Sr.[11,12] One indeed observes, like for these oxides, a doubling of the periodicity along $\vec{a}$, suggesting that it is associated with charge-orbital ordering. This feature is strongly supported by the HREM study, which shows a system of double stripes, which can be attributed to two kinds of manganese octahedra. However, it differs from all other manganites by the presence of a second direction of modulation, involving a doubling of the periodicity along $\vec{b}$. Note that such a quadrupling of the b_p axis was also observed for the *Pnma*-type perovskite $La_{7/8}Sr_{1/8}MnO_3$.[19]

The second important feature concerns its X-ray study, which does not evidence any superstructure at low temperature but shows the existence of high anisotropic displacement parameters of the oxygen atoms that we assume to be correlated to the rather strong displacements detected in the HREM images. This suggests a displacive modulation, slowly evolving with T and correlated to an ordering of the oxygen atoms, which cannot be detected from XRPD measurements.

Thus, from these observations, we believe that both charge-orbital ordering and displacive ordering of the oxygen atoms take place in $Bi_{2/3}Sr_{1/3}MnO_3$ and are correlated. A neutron diffraction study is absolutely required to shed light on these phenomena.

CM021309F

(19) Yamada, Y.; Hino, O.; Nohdo, S.; Kanao, R.; Inami, T.; Katano, S. *Phys. Rev. Lett.* **1996**, *77*, 904.